Hindawi
Mobile Information Systems
Volume 2022, Article ID 8075611, 12 pages
https://doi.org/10.1155/2022/8075611

Research Article

Deformation Monitoring and Spatiotemporal Evolution of Mining Area with Unmanned Aerial Vehicle and D-InSAR Technology

Hao Tan,[1,2] **Xuexiang Yu**,[3] **Mingfei Zhu**,[2] **Zhongchen Guo**,[2] **and Hengzhi Chen**[4]

[1]*State Key Laboratory of Mining Response and Disaster Prevention and Control in Deep Coal Mines, Anhui University of Science and Technology, Huainan 232001, China*
[2]*School of Earth and Environment, Anhui University of Science and Technology, Huainan 232001, China*
[3]*School of Geomatics, Anhui University of Science and Technology, Huainan 232001, China*
[4]*Jiangsu Wisdom Spatial Geographic Information Technology Co LTD, Nanjing 211899, China*

Correspondence should be addressed to Hao Tan; 2021217@aust.edu.cn

Received 25 March 2022; Revised 22 April 2022; Accepted 5 May 2022; Published 20 May 2022

Academic Editor: M. Praveen Kumar Reddy

The extraction of underground mineral sources has a significant negative impact on the local environment, results in land surface subsidence. As far as subsidence monitoring technology is concerned, leveling is the most accurate. However, leveling can only obtain discrete point data but not the whole area information of the subsidence basin. In this study, Differential Interferometric Synthetic Aperture Radar (D-InSAR) combined with Unmanned Aerial Vehicle (UAV) technology is used to study the subsidence characteristics of the whole working panel. In this analysis, the Huainan mining area is tested as a research area; measured data are compared to the elevation accuracy of the Digital Surface Model (DSM) data, which can be considered for the subsequent works of the mining area. Based on the subsidence affected area, the ground object-type information is recorded to provide basic information for the ecological restoration work after mining so that the data before and after mining can be obtained synchronously. Finally, the differential interference results and Digital Orthophoto Map (DOM) data are combined to assess the spatiotemporal evolution of working panel subsidence and its influence on surface features. The main novelty of the proposed work is combining UAV and D-InSAR to get more accurate analysis of mining subsidence. It can be done using the proposed method.

1. Introduction

The depletion of land resources caused by coal mining is a well-known issue around the world. Surface buildings, water bodies, and roadways are all harmed when collapse pits, fissures, and subsidence steps develop. This has a significant impact on the residents of the mining area's health and quality of life [1, 2]. Therefore, real-time and high-precision monitoring, prediction, and early warning of land surface disasters are critical for safe and efficient production as well as environmental protection in mining areas [3–5].

The conventional method of monitoring is to place observation stations in the form of discrete points along the working surface's trend and inclination lines, establishing a monitoring mode with "points" as "lines" and "lines" as "polygons" [6, 7]. Despite its excellent precision, the limited monitoring scope, low efficiency, big workload, and expensive cost cannot be overlooked [8–10]. Simultaneously, this monitoring mode lowers the dependability of monitoring the entire mining face [11, 12]. The D-InSAR technique is used to synthesize elevation maps and get surface deformation differences over time, and it has the advantage of being available 24 hrs a day, on a large scale under any climatic conditions [13–16]. It is widely employed in monitoring the subsidence evolution in mining areas such as coal mines [17–20]. The subsidence of the land surface in the mining area, however, is large due to the radar wavelength limitation, and the land surface subsidence suppresses the monitoring threshold of the D-InSAR technique during the return visit time interval, generating phase unwrapping errors. Therefore, it is difficult to compute the land surface subsidence of two periods adequately [21, 22]. The InSAR method, on the contrary, mainly records the land surface elevation value, which does

not reflect the properties and scope of surface objects such as agriculture, buildings, and highways. Moreover, the InSAR time-series approach's potential is frequently limited by a lack of artificial objects and sparse vegetation cover, which makes acquiring deformation characteristics more difficult due to a lack of observation stations[23], particularly in the mine zone.

The UAV tilt photogrammetry technique can be well utilized to obtain the Digital Surface Model (DSM) and Digital Orthophoto Map (DOM) through optical photos imaging [24]. It is not limited by wavelength or other parameters, and it can monitor and observe the surface subsidence of the mining area. Mining subsidence monitoring has steadily been a research priority. For example, Ignjatović Stupar et al. [25] used the Velenje coal mine as a research area and collected observation data in 2017 by using a combination of the total station (TS) method, the Global Navigation Satellite System (GNSS), and Unmanned Aerial Vehicle (UAV) technologies. In this study, the height difference of reference points was evaluated using statistical analysis and test techniques of similar observations. Furthermore, utilizing the ultra-high-resolution normal perforation approach, Puniach et al. [26] provided a process for the automatic calculation of the horizontal displacement field in underground mining. The approach of using the UAV photogrammetry technique to monitor the dynamic land surface subsidence basin caused by underground coal mining and produce mining subsidence characteristics in a short time was presented by Dawei et al. [27].

The influence of terrain variations on image resolution, photo overlap degree, and monitoring accuracy was examined [28]. Then, they attached a TOF sensor to the UAV and set a programmed PID controller code to keep it flying at the same height above the ground, effectively realizing the UAV following monitoring. The UAV technique achieves elevation accuracy of roughly 50 mm in mining areas with difficult topography and around 30 mm in flat terrain areas. The accuracy of the elevation value obtained by the UAV technique is lower than that of the initial stage due to the small amount of subsidence, whereas the accuracy of the small deformation value obtained by the D-InSAR technique is less than 10 mm due to the small amount of subsidence at the initial stage [29, 30]. Based on the advantages of the above two technologies, the study proposes a four-step procedure as below:

(1) Because land surface deformation is minor early in the mining process, D-InSAR technology is used to monitor the subsidence of the mining area, record the surface deformation information, and assess the extent of subsidence influence.

(2) The RTK and UAV techniques are performed to obtain the surface deformation information, respectively. The accuracy of the data obtained by the two technologies are compared with the measured leveling data. It has been established that the elevation data obtained by the UAV technique can meet the needs of subsidence monitoring parameter inversion in the mining area.

(3) Overall mining demand planning before and after mining, as well as the collection of surface object type information and statistics during subsidence monitoring, are all important data sources for ecological restoration of the mining subsidence area after mining.

(4) Combining the data of UAV and D-InSAR techniques, the vertical deformation image obtained from SAR data is combined with DOM to reveal the spatiotemporal subsidence evolution of the mine area.

An enhanced phase optimization approach integrating UAV and D-InSAR is provided in response to the aforementioned difficulties. The research region is the subsidence area in the Huainan mining area in China, and this method is used to process SAR and UAV data covering the study area. The evolution of surface subsidence in the mining area is then indicated by obtaining deformation in the mining area. The final results of the synthesized study point to the possibility of identifying potential dangers and developing additional strategies to reduce the impact of mining regions on the environment and resources.

2. Materials and Methods

2.1. Study Area. The Banji coal mine is located at the intersection of Lixin County, Yingshang County, and Yingdong District, China. In the context of administrative division, it belongs to Huji Town, Lixin County, and Bozhou City. The minefield is situated 25 km north of Lixin County and 30 km south of Yingshang County. The study area extends between longitudes 116° 09E′ and 116° 30′ E and latitudes 32o51′ N 32° 56′ N, covering an area of 3358.84 km^2 (Figure 1). The land cover/land use of the mine area is characterized by dry land, arbor forest land, other forest lands, mining land, rural homestead, railway land, highway land, rural roads, river water surface, pit and pond water surface, ditches, idle land, and agricultural lands.

The Banji mine's capital construction stage runs from 2019 to 2020. On April 5, 2021, mining in the study area commenced. The Dongyi mining region, with a strike line length of 1070 meters, a dip line length of 270 meters, and recoverable deposits of 940000 tonnes, is the first planned mining area. According to the information, there are 36 boreholes in the research area of the Banji mine. The loose layer thickness in the monitoring area is 500 m to 648 m with an average of 600 m. The overlying bedrock thickness ranges from 30 m to 330 m, with an average of 130 m and the coal seam floor mining depth ranges from 646 m to 876 m, with an average of 786 m. The working area has the characteristics of a thick loose layer, significant mining depth, and thin bedrock in general. The mine has no operating panel mining history and no mining subsidence area to date.

2.2. UAV Data Acquisition and Processing. The Saier 102s five-lens camera on the Dajiang M300 four-rotor UAV can collect and shoot image information from five different

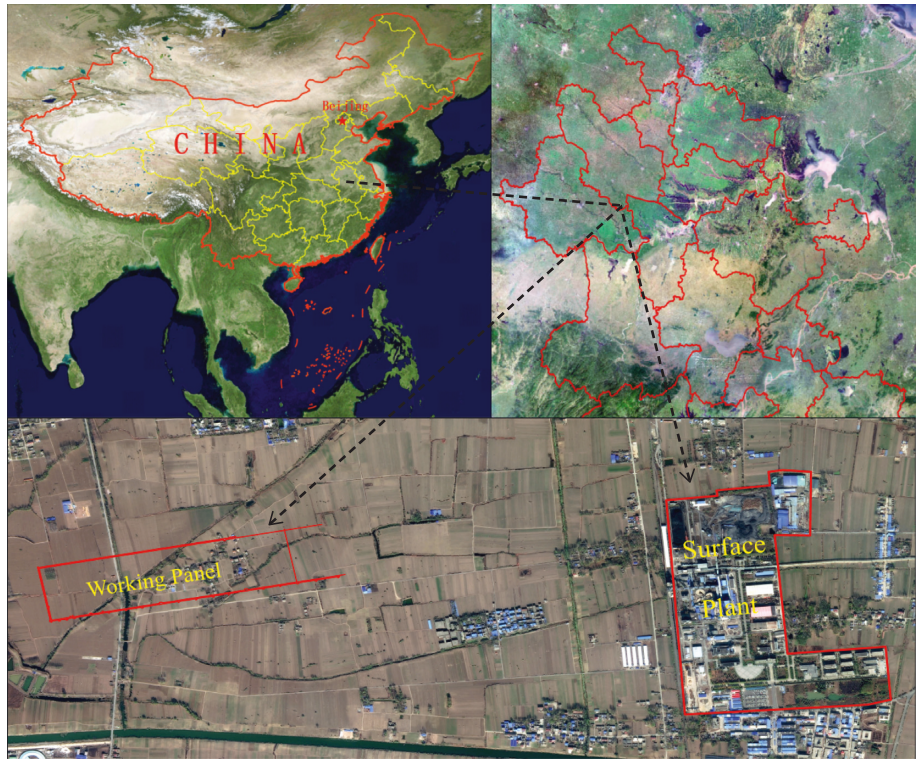

Figure 1: The geographical location maps of the study area (110801 working panel).

directions: vertical, front view, rear view, left view, and right view. As a result, obtaining the essential data are more convenient. Table 1 lists the major characteristics of the UAV and camera.

The study area's intervisibility and light intensity were assessed to be good during the field assessment. Roads, wheat-growing fields, buildings, trees, and other land objects on the land surface. Leveling and RTK observation stations are mainly distributed on the side of the path or ditch system. Individual observation points near the wheat field are excluded based on the DOM and field observation. The other points can be used to confirm the tilt photogrammetry's elevation correctness.

Based on an S-shaped total flight path, with respect to the study area, a 2.0 km^2 region was included. Before flying, the UAV must uniformly distribute the image control points based on the route's range and the actual geomorphological features and then utilize RTK to collect the image control points' 3D coordinates. At the same time, the RTK and leveling data of monitoring points are collected before and after the flight. The number of photographs collected was 17650 and 17695, respectively.

2.3. Methods

2.3.1. SAR Data Processing. The European Space Agency (ESA) provided the Sentinel-1A (S1A) products, which were processed to execute the following corrections and enhancements: multilooking and terrain adjustments, as well as calculating phase differences and D-InSAR data. To generate the deformation image, the SLC subswaths were divided and debursted independently before completing the coherence phase and vertical deformation using two different date images (e.g., May 11, 2021–May 23, 2021; May 23, 2021–June 4, 2021; June 16, 2021–June 28, 2021; June 21, 2021–July 3, 2021). Finally, the obtained images were multilooked and projected using a digital elevation model (DEM) acquired from the Shuttle Radar Topography Mission (SRTM) and a Universal Transverse Mercator (UTM) coordinates system of data from the World Geodetic System 1984 (WG84) to perform terrain correction.

To acquire the LOS deformation value and decompose it to obtain the vertical subsidence value for periodic monitoring, the double-track approach was employed. Because of the area's unique location, there are three types of SAR data coverage, two of which can be employed to reduce SAR data monitoring time.

2.3.2. UAV Photo Acquisition Process. The most common methods of data processing are data import, aero triangulation, prickles, and coordinate system transformation, among others. Osgb format 3D models, DOM, and DSM are the products.

2.3.3. Data Accuracy Verification. The accuracy of UAV tilt photogrammetry is verified by combining Real-Time Kinematic (RTK) data and leveling data collected in the field, namely, plane coordinates (x, y), and elevation.

2.3.4. Land Surface Statistics and Spatiotemporal Law Analysis. Land conditions can be gathered using the collaborative monitoring mode of SAR data and the UAV tilt

Table 1: UAV and camera parameters.

Flight speed	Flight altitude	Wind resistance	Lens number	Effective pixels	Image resolution	Course overlap ratio (%)	Lateral overlap rate (%)
13 m/s	150 m	Level 7	5	Total 120 million pixels	2.2 cm	80	70

photogrammetry technique to provide basic information for postmining ecological restoration. The process of subsidence at the initial mining stage is investigated, and the spatio-temporal evolution operation of subsidence for mining is obtained. Figure 2 depicts the major experimental procedure.

3. Results

3.1. Model Building. DOM, DSM, and 3D model of mining area are generated (Figure 3). The obtained DOM has the characteristics of geometric map accuracy and image features, high accuracy, rich information, intuitive truth, and a short production cycle that can reflect the surface object information of a mining area truly and effectively. The DSM includes elevation information of surface buildings, trees, roads, fields, and other ground objects, which most truly reflects surface fluctuation features. Compared with DEM, the table features are more detailed [31].

Figure 3 shows the 3D model of the mining area. The actual landform features can be seen in the 3D model of the mining area, with an image size of 91175×63554 and a resolution ratio of 22 cm.

3.2. Plane Coordinate Accuracy Verification. Figure 4(a) depicts the horizontal and RTK monitoring points distribution. The black box represents the working panel position, the red triangle represents the monitoring points arranged along the dip line, and the yellow five-pointed star represents the observation points along the strike line, all of which conforms to the mining area's subsidence monitoring point distribution criterion. One by one, examine the matching effects of leveling observation stations and points on the DOM graph. The schematic representation of the matching degree of observation stations randomly picked from the dip line and strike line is shown in Figures 4(b) and 4(c), demonstrating that the plane coordinate of DOM has a high-precision intuitively.

To verify the plane accuracy of UAV tilt photography, 7 and 19 verification points were set on the road along the strike line and the dip line of the working face, respectively, with an average interval of 80 meters between each verification point (Figure 4(d)). The verification points of the strike line were represented by a yellow five-pointed star, while the verification points of the dip line were represented by a red triangle. The root mean square errors (RMSEs) of x and y coordinates of the verification points are shown in Table 2. Because the road condition in the trend direction is poor, the accuracy of the verification point is slightly lower than that of the verification point. The road in the trending direction, on the other hand, is a cement road in good condition.

3.3. Elevation Accuracy Verification. The elevation values of leveling observation stations in the two directions of the strike line and dip line are extracted from the first phase and compared to RTK and leveling data. Figure 5 depicts the accuracy analysis of RTK data collected in the field and matching DSM land surface point elevation values. The [[parms resize(1),pos(50,50),size(200,200),bgcol(156)]] verified with leveling data. The precision of the dip line's pointing accuracy is distributed within 5 cm, as shown in Figure 6(b). MS29, MS50, and MS56 have absolute errors of more than 10 cm, with MS56 having a 26 cm anomaly. The surrounding wheat seedlings may be close to the point, affecting the point's elevation value, which can be removed based on the DOM image.

The accuracy of UAV tilt photogrammetry is verified by comparing DSM elevation and measured leveling value, as shown in Figures 6(c) and 6(d). The strike line elevation absolute errors are 0.04 cm and 8.62 cm, respectively. All other sites are within 5 cm except for MLA076, which is 8.62 cm, and MLA074, which is 6.78 cm. Absolute dip line elevation errors are 0.04 cm and 13.59 cm, respectively. MS29 has an absolute error of 13.59 cm, MS50 has an absolute error of 9.33 cm, MS40 has an absolute error of 5.77 cm, and MS46 has an absolute error of 5.66 cm.

After comparing DSM elevation and leveling values, preliminary verification shows that MLA015-MLA039 points have accepted accuracy.

As demonstrated in Table 3, it can be seen from the comparison of root mean square error among all data that the root mean square error of DSM, RTK, and leveling data is smaller on the trend line. On the strike line, the root mean square error between DSM elevation value and RTK data is considerable, while between DSM elevation value and leveling data, the root mean square error is the modest. As a result, it is possible that the surrounding environment has an impact on RTK data from the MLA015-MLA039 observation stations.

Overall, as compared to RTK data, the accuracy of DSM obtained by UAV tilt photogrammetry can approach within 5 cm in elevation, and its error is lower. The overall accuracy is fairly consistent, which is sufficient for mining area parameter inversion.

On the ground of the mining area, a real-time dynamic monitoring system with one reference station (BJCMP) and twelve real-time monitoring stations has been created. On the top of an office building in the industrial square, the reference station is positioned. Near the air, the shaft is a real-time monitoring station (MCORS01). At the intersection of the 110801 study area's strike and dip observation lines, one real-time monitoring stations is set up (MCORS02). Figure 7 depicts the distribution of real-time monitoring stations.

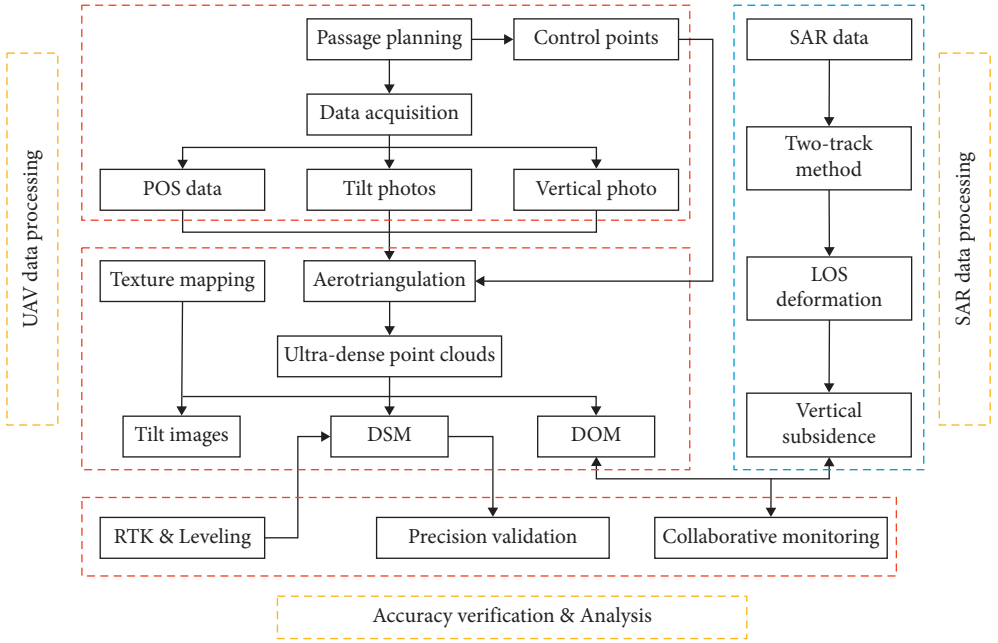

Figure 2: Flowchart of the data and experiments adopted in the present study.

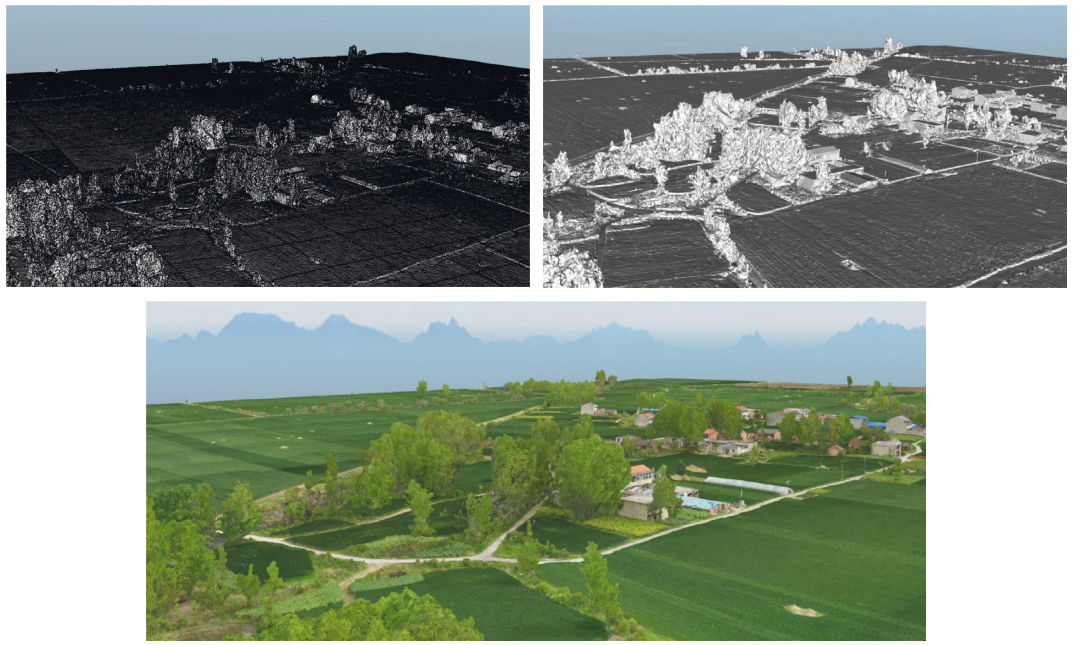

Figure 3: Generated 3D digital models of the present study area.

The elevation data of MLA015 and MLA039 were collected in the first phase by connecting the Qianxun base station, which could be influenced by the surrounding environment and cause errors. In the second experiment, the RTK1 + 2 mode was used, with a reference station and two mobile data collection stations mounted on the mining area's office roof. The reference station on the mining area's office roof is shown by the red five-pointed star in Figure 7.

The error analysis diagram of the verification points on the road in the two strike and dip directions is taken as illustrated in Figure 8. The strike for rammed land roads is set at 7 points, and the dip for cement (asphaltic) roads is set at 19 points, with an average distance of 80 meters between the two points. In Figure 8(a), the elevation difference is mostly within 5 cm, with the exception of the JC9 point, which is 6.29 cm. In Figure 8(b), the difference in the JC20 point difference is 5.72 cm, while the other locations are all within 5 cm. The root mean square error of the cement road (dip) monitoring point is 2.15 cm, and the RMSEs of the tamped land road (strike) monitoring point is 3.71 cm, as shown in Table 4, essentially meeting the requirements of mining subsidence parameter inversion.

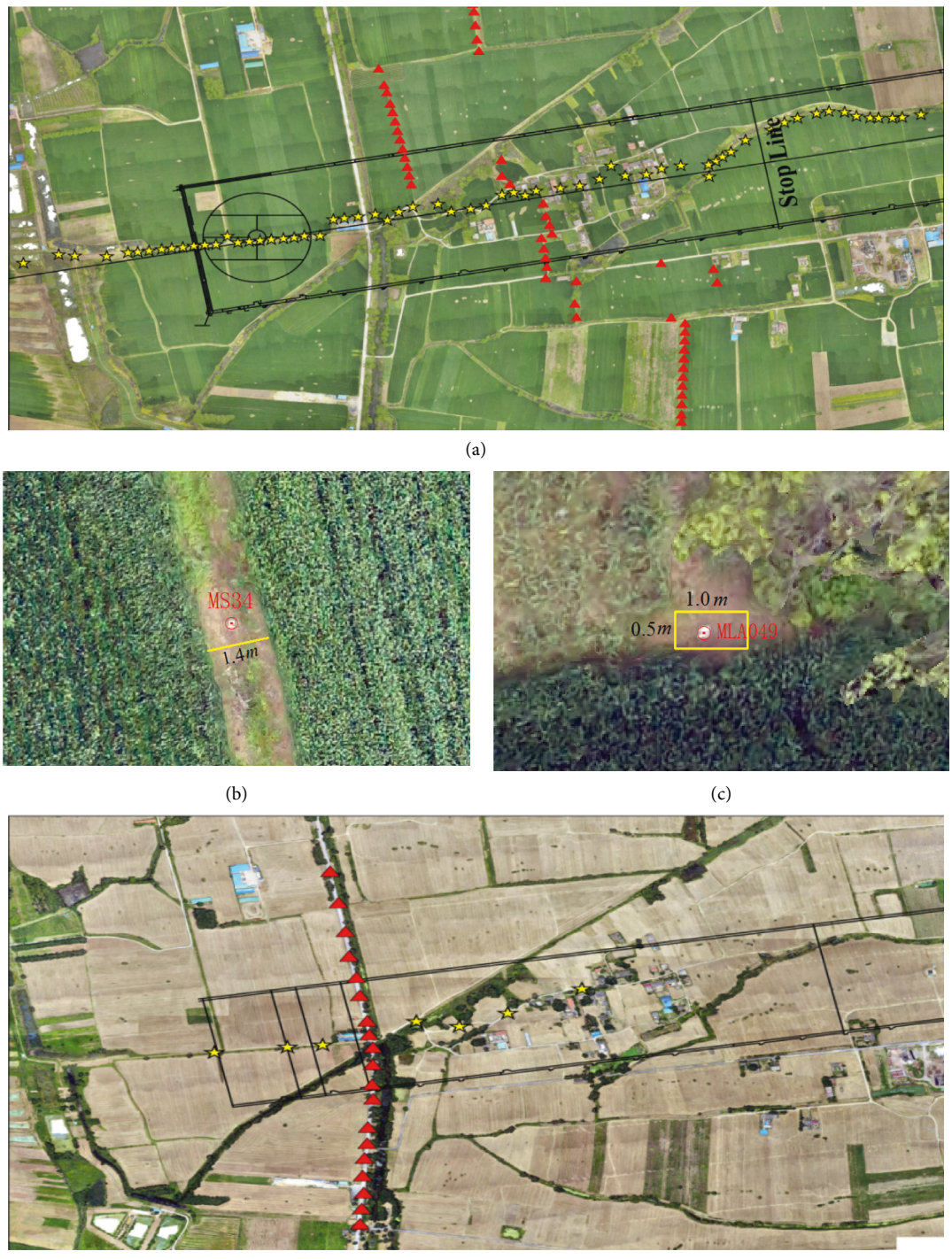

(a)

(b)

(c)

(d)

Figure 4: Distribution of monitoring points and verification points in the mining area: (a) station distribution; (b) dip line observatory; (c) strike line observation station; (d) distribution of verification points.

Table 2: Coordinate accuracy analysis.

Orientation	Coordinates	RMSE cm
Strike line	x	3.45
	y	2.21
Dip line	x	1.75
	y	2.61

4. Discussion

4.1. Workface Influence Range and Land Category Statistics. The D-InSAR technique allowed monitoring of small deformations, and subsidence or collapse of the mining area due to minimal subsidence at the beginning of mining [32]. As a result, based on the surface deformation range and

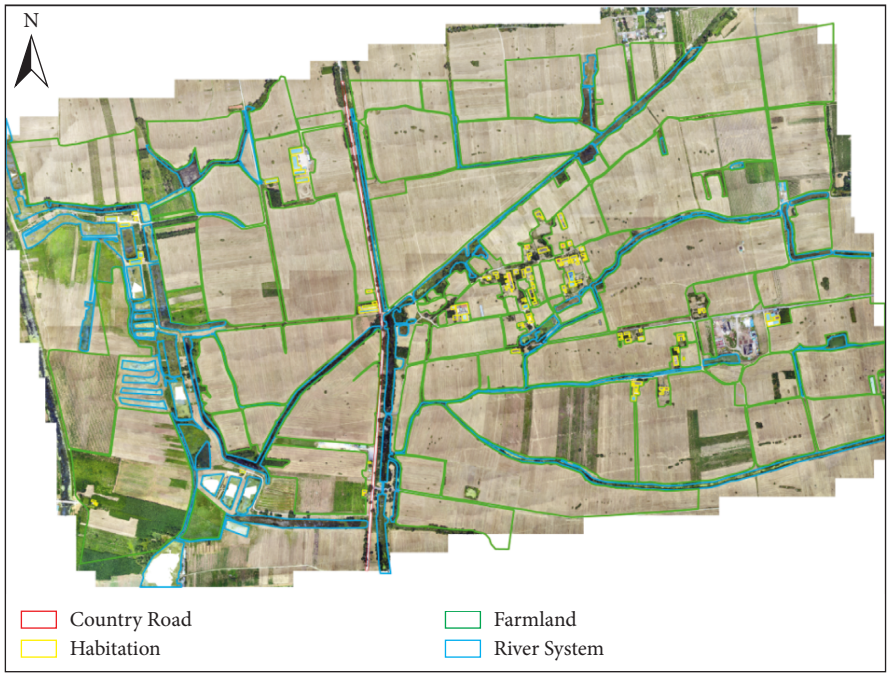

Figure 5: Vector map of the impacts of mining activities.

geological and mining conditions obtained from SAR data, the influence range of the mining research area was defined at 600 meters outward expansion on both sides of the strike direction and 400 meters outward expansion on both sides of the dip. Ground objects such as buildings, crops, roads, and water systems have been damaged.

Table 5 shows that 98 houses totaling 1.42 hectares were statistically affected. The total size of the farmland area is 186.03 hectares. The main road is County Road 046, which is 1.33 km long and covers 0.77 hectares. The water system consists mainly of fish ponds and ditches, which cover a total of 20.78 hectares. As demonstrated in Figure 5, the statistical results can provide basic information for postmining ecological restoration.

4.2. Temporal and Spatial Analysis. The land surface movement law of thick alluvium has been the subject of numerous research studies [33] with the majority of them focused on numerical simulation, similar material simulation, and observed strike and dip line data. The mobile communication has powerful data processing capabilities for accurately revealing land surface dynamic changes in a short time [34–37]. In terms of numerical simulation and comparable material simulation, these two methods are subject to some uncertainty, and there will be a gap between them and reality. The profile line formed by the discrete data from strike and dip line observation stations is insufficient for analyzing the temporal and spatial evolution law of mining subsidence in the form of area. Conventional methods cannot actually and intuitively illustrate the influence range of surface subsidence and the temporal and spatial evolution law of mining subsidence [38–42].

The differential interferogram during the two periods of Sentinel-1 SAR data is shown in the left side of Figure 9. The three-dimensional depiction of the subsidence influence range is displayed on the right side. It is depicted as expanding the subsidence to 25 times due to the modest subsidence effects. In Figure 9(d) the solid black line indicates the range of subsidence of less than 20 mm, and the solid yellow line shows the range of subsidence of less than 40 mm. On April 7, 2021, the working face begins mining, and on May 24, 2021, June 4, 2021, and June 23, 2021, the mining progress is 115.5 m, 157 m, and 232.5 m, respectively. This reveals that the D-InSAR technique has the capability to reveal the minimal and large amount of land surface deformation observation data [43, 44].

From May 11, 2021, to May 23, 2021, the central area does not reach County Road 046; during the period of May 23, 2021 to June 4, 2021, the main influence area is extended to County Road 046. In addition, during the period from June 16, 2021 to June 28, 2021 and from June 21, 2021 to July 3, 2021, the main influence area is extended to the east side of County Road 046. It can be observed that the mining subsidence area expands in the mining direction between two dates. In the early mining stage Figure 9(a), the image of land surface changes expands to reveal the minimal changes. In this image, the convergence at the boundary is very slow and reveals a long-term slight subsidence zone. The surface deformation value is small and displays the subsidence basin in an elliptical to circular form, with symmetry on both sides of the dip and asymmetry on both sides of the strike. The subsidence area reaches its mamima in the center, and the elliptical subsidence basin becomes nearly rounded. Figures 9(c) and 9(d) revealed that the, the main subsidence area is nearly rounded form, with symmetrical development on both sides of strike and dip that reveals subsidence

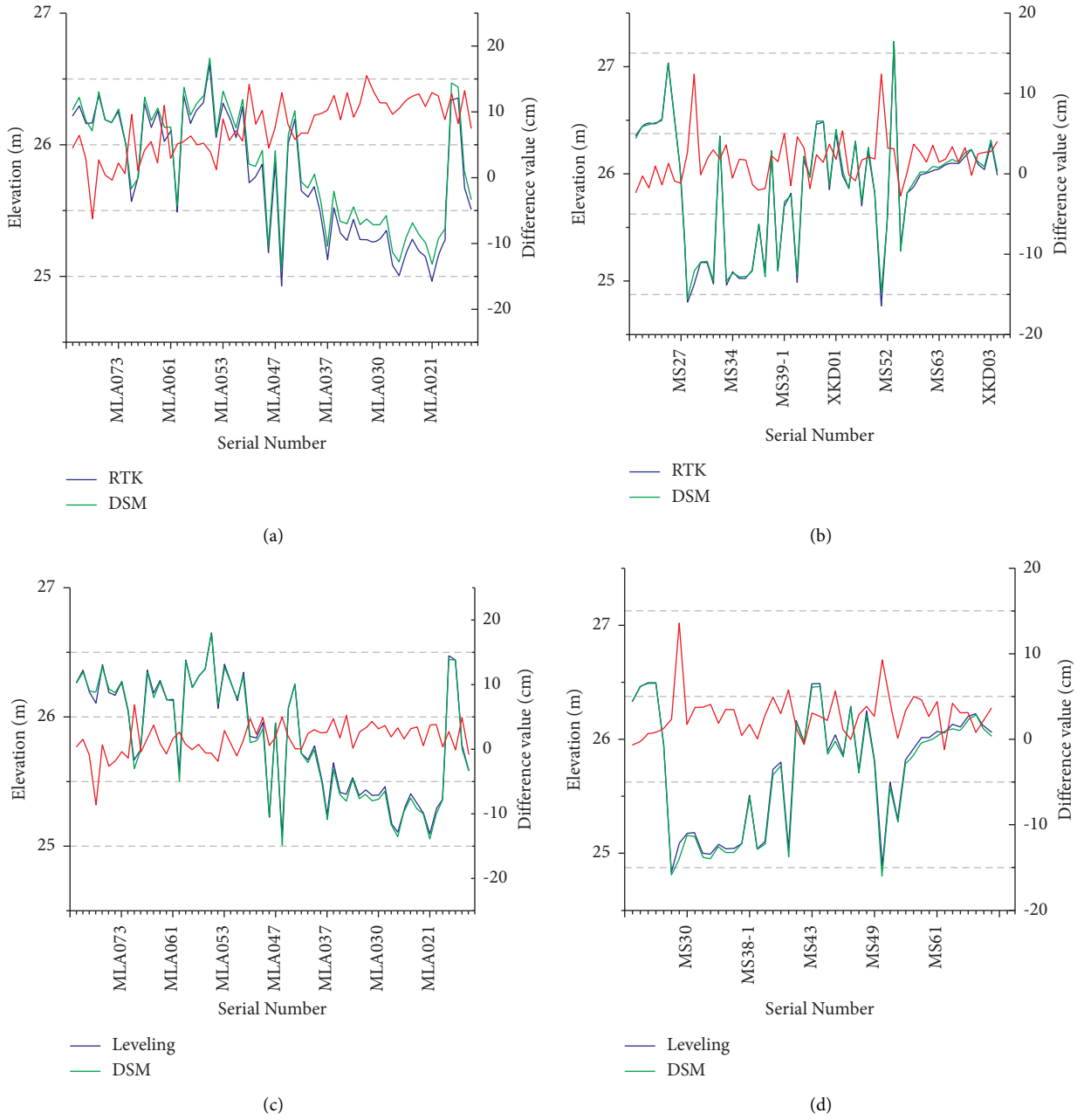

Figure 6: Comparison of leveling, RTK, and DSM elevation: (a) strike line accuracy verification; (b) dip line accuracy verification; (c) strike line accuracy verification; (d) dip line accuracy verification.

Table 3: Comparison of data RMSE.

Data type	Orientation	RMSE (cm)
DSM and RTK	Strike line	8.78
	Dip line	3.53
DSM & leveling	Strike line	2.85
	Dip line	3.81
RTK & leveling	Strike line	6.74
	Dip line	1.79

positively related to mining extraction., The overall subsidence of the land surface Figures 9(a)–9(c) is dominant, and the subsidence in the middle is not cleary apparent, but the solid yellow line area has large surface deformation showing the characteristics of a concentrated subsidence Figure 9(d).

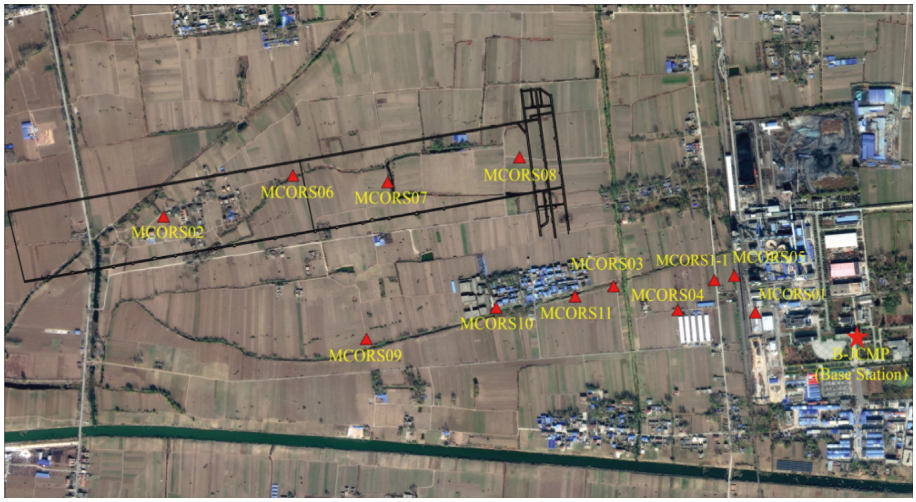

Figure 7: Distribution map of real-time monitoring stations.

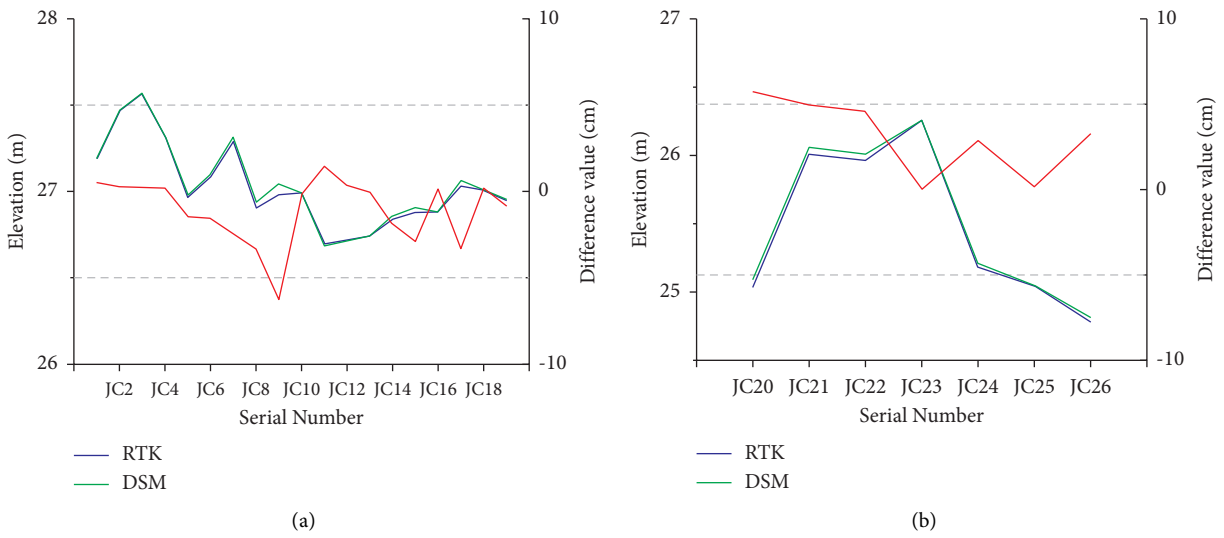

Figure 8: Road elevation accuracy verification: (a) dip line accuracy verification; (b) strike line accuracy verification.

Table 4: Comparison of RMSEs of road monitoring points.

Data type	Orientation	RMSE (cm)
DSM and RTK	Strike line	3.71
	Dip line	2.15

Table 5: Land-type statistics.

Land types	Area (hm^2)
Building	1.42
Farmland	186.03
Road	0.77
Drainage	20.78

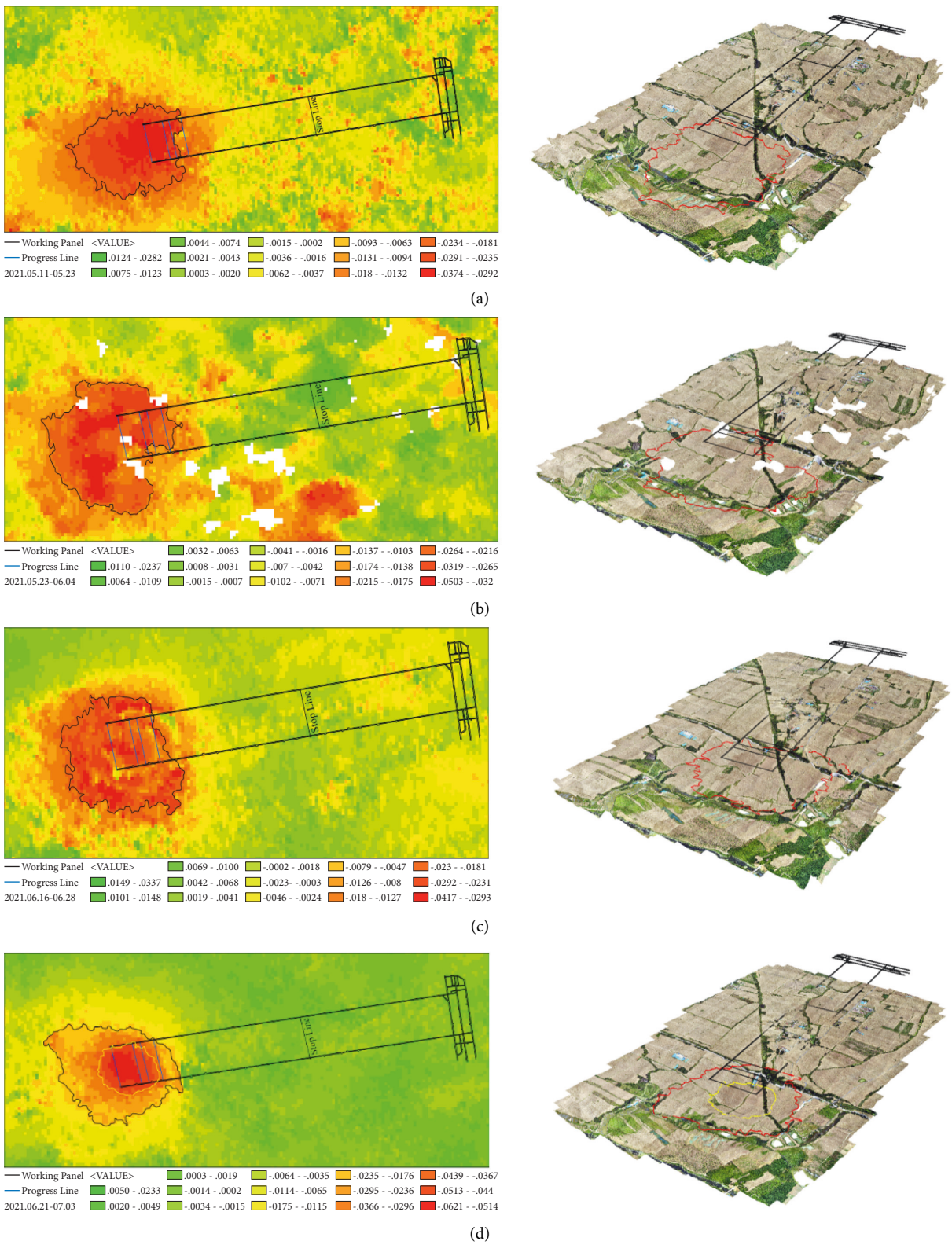

Figure 9: Spatial-temporal evolution of land surface subsidence beneath thick alluvium deposits: (a) May 11, 2021–May 23, 2021; (b) May 23, 2021–June 4, 2021; (c) June 16, 2021–June 28, 2021; (d) June 21, 2021–July 3, 2021.

Thus, its monitoring is essential for the safety and economics of coal mining [45, 46]. Therefore, risk assessment and management of coal mining using spatiotemporal mobile imaging systems is extremely important for sustainable development [47].

5. Conclusion

In this study, the DOM, DSM, and 3D model of the surface of the mining area working face panel are obtained based on the UAV tilt photogrammetry technique to better reveal the subsidence law in the mining area of Banji coal mine, China. The elevation values extracted by DSM, RTK elevation data, and leveling data are compared in pairs based on the evening process. The accuracy of RTK data is significantly different due to the influence of the surrounding environment. UAV tilt photogrammetry data provides a higher level of stability than RTK data, making it suitable for parameter inversion and subsidence prediction.

The processed SAR data derived from Sentinel-1 data provided information on the subsidence of the working panel on a regular basis; however, it cannot reflect the land surface characteristics and geomorphic features. The influence range and degree of the retreating progress on the surface features are analyzed on the unified scale of space and time by combining the SAR data with the DOM data from the mining area.

Integrate leveling data, RTK, SAR, DOM, DSM, and 3D model data generated by UAV tilt photogrammetry allowed us to reveal the subsidence law of the working panel in the whole basin on a unified scale of space and time. It has been realized that monitoring discrete points forming a linear form to a 3D + time scale allows providing a basis for the comprehensive study of the mining subsidence law.

Overall, this study verified the accuracy of DSM. In the future, Data will be upgraded in the future to allow for parameter inversion of the mining area, mining forecast of the working panel, and a more adequate database for postmining ecological restoration work.

Data Availability

The data used to support the findings of this study are included within the article.

Conflicts of Interest

The authors declare that they have no conflicts of interest.

Acknowledgments

This project was supported by the Key Research and Development Program of Anhui Province (Grant no. 202104a07020014) and the Major Science and Technology Project of Anhui Province (Grant no. 202103a05020026).

References

[1] W. Guo, M. Guo, Y. Tan, E. Bai, and G. Zhao, "Sustainable development of resources and the environment: mining-induced eco-geological environmental damage and mitigation measures-A case study in the henan coal mining area, China," *Sustainability*, vol. 11, no. 16, p. 4366, 2019.

[2] Y. Wang, X. Wu, S. He, and R. Niu, "Eco-environmental assessment model of the mining area in Gongyi, China," *Scientific Reports*, vol. 11, no. 1, p. 17549, 2021.

[3] L. Wang, K. Deng, H. Fan, and F. Zhou, "Monitoring of large-scale deformation in mining areas using sub-band InSAR and the probability integral fusion method," *International Journal of Remote Sensing*, vol. 40, no. 7, pp. 2602–2622, 2019.

[4] J. Huang, K. Deng, H. Fan, and S. Yan, "An improved pixel-tracking method for monitoring mining subsidence," *Remote Sensing Letters*, vol. 7, no. 8, pp. 731–740, 2016.

[5] S. G. Ishwar and D. Kumar, "Application of DInSAR in mine surface subsidence monitoring and prediction," *Current Science*, vol. 112, no. 1, p. 46, 2017.

[6] L. Chen, L. Zhang, Y. Tang, and H. Zhang, "Analysis OF mining-induced subsidence prediction BY exponent knothe model combined with insar and leveling," *ISPRS Annals of the Photogrammetry, Remote Sensing and Spatial Information Sciences*, vol. IV-3, pp. 53–59, 2018.

[7] M. Zheng, K. Deng, H. Fan, and S. Du, "Monitoring and analysis of surface deformation in mining area based on InSAR and GRACE," *Remote Sensing*, vol. 10, no. 9, p. 1392, 2018.

[8] J. Zhu, Z. Yang, and Z. Li, "Recent progress in retrieving and predicting mining-induced 3D displacement using InSAR," *Acta Geodaetica et Cartographica Sinica*, vol. 48, no. 2, pp. 135–144, 2019.

[9] H. Fan, X. Gao, J. Yang, K. Deng, and Y. Yu, "Monitoring mining subsidence using A combination of phase-stacking and offset-tracking methods," *Remote Sensing*, vol. 7, no. 7, pp. 9166–9183, 2015.

[10] J. Huang, K. Deng, H. Fan, S. Lei, S. Yan, and L. Wang, "An improved adaptive template size pixel-tracking method for monitoring large-gradient mining subsidence," *Journal of Sensors*, vol. 2017, Article ID 3059159, 11 pages, 2017.

[11] Z. F. Yang, Z. W. Li, J. J. Zhu, J. Hu, Y. J. Wang, and G. L. Chen, "Insar-based model parameter estimation of probability integral method and its application for predicting mining-induced horizontal and vertical displacements," *IEEE Transactions on Geoscience and Remote Sensing*, vol. 54, no. 8, pp. 4818–4832, 2016.

[12] Z. Yang, H. Yi, J. Jian, W. Zhi, J. Su, and Q. Liu, "Spatio-temporal evolution law analysis of whole mining subsidence basin based on InSAR-derived time-series deformation," *Chinese Journal of Nonferrous Metals*, vol. 07, pp. 1515–1522, 2016.

[13] H. A. Zebker and R. M. Goldstein, "Topographic mapping from interferometric synthetic aperture radar observations," *Journal of Geophysical Research*, vol. 91, no. B5, p. 4993, 1986.

[14] A. K. Gabriel, H. A. Zebker, and H. A. Zebker, "Mapping small elevation changes over large areas: differential radar interferometry," *Journal of Geophysical Research*, vol. 94, no. B7, pp. 9183–9191, 1989.

[15] A. Gaber, M. Abdelkareem, I. Abdelsadek, M. Koch, and F. El-Baz, "Using InSAR coherence for investigating the interplay of fluvial and aeolian features in arid lands: implications for groundwater potential in Egypt," *Remote Sensing*, vol. 10, no. 6, p. 832, 2018.

[16] M. Abdelkareem, A. Gaber, F. Abdalla, and G. K. El-Din, "Use of optical and radar remote sensing satellites for identifying and monitoring active/inactive landforms in the driest desert in Saudi Arabia," *Geomorphology*, vol. 362, Article ID 107197, 2020.

[17] M. Li, L. Zhang, M. Liao, and X. Shi, "Detection of coal-mining-induced subsidence and mapping of the resulting deformation using time series of ALOS-PALSAR data," *Remote Sensing Letters*, vol. 7, no. 9, pp. 855–864, 2016.

[18] Y. Lu, C. Q. Ke, D. L. Chen, and M. He, "Applocation of PS-InSAR in pei county mining area surface subsidence monitoring," *Geospatial Inf*, vol. 14, no. 5, pp. 96–99, 2016.

[19] L. Dong, C. Wang, Y. Tang et al., "Time series InSAR three-dimensional displacement inversion model of coal mining areas based on symmetrical features of mining subsidence," *Remote Sensing*, vol. 13, no. 11, p. 2143, 2021.

[20] Y. Du, S. Yan, F. Zhao, D. Chen, and H. Zhang, "DS-InSAR based long-term deformation pattern analysis in the mining region with an improved phase optimization algorithm," *Frontiers in Environmental Science*, vol. 10, 2022.

[21] C. W. Chen and H. A. Zebker, "Phase unwrapping for large SAR interferograms: statistical segmentation and generalized network models," *IEEE Transactions on Geoscience and Remote Sensing*, vol. 40, no. 8, pp. 1709–1719, 2002.

[22] M. Jiang, Z. Li, X. Ding, J. Zhu, and H. Yin, "A study on the maximum and minimum detectable deformation gradients resolved by InSAR," *Chinese Journal of Geophysics*, vol. 52, no. 7, pp. 1715–1724, 2009.

[23] Z. Zhang, J. Wang, C. Tang, Q. Y. Fu, and H. Zhang, "Subsidence monitoring in coal area using time-series InSAR combining persistent scatterers and distributed scatterers," *Int. J. Appl. Earth Observations Geoinformation*, vol. 39, no. 99, pp. 1–11, 2015.

[24] P. K. R. Maddikunta, S. Hakak, M. Alazab et al., "Unmanned aerial vehicles in smart agriculture: applications, requirements and challenges," 2007, https://arxiv.org/abs/2007.12874.

[25] D. Ignjatović Stupar, J. Rošer, and M. Vulić, "Investigation of unmanned aerial vehicles-based photogrammetry for large mine subsidence monitoring," *Minerals*, vol. 10, no. 2, p. 196, 2020.

[26] E. Puniach, W. Gruszczyński, P. Ćwiąkała, and W. Matwij, "Application of uav-based orthomosaics for determination of horizontal displacement caused by underground mining," *ISPRS Journal of Photogrammetry and Remote Sensing*, vol. 174, pp. 282–303, 2021.

[27] Z. Dawei, Q. Lizhuang, Z. Demin, Z. Baohui, and G. Lianglin, "Unmanned aerial vehicle (uav) photogrammetry technology for dynamic mining subsidence monitoring and parameter inversion: a case study in China," *IEEE Access*, vol. 8, pp. 16372–16386, 2020.

[28] X. Yang, W. Yao, J. Zheng, B. Ma, and X. Ma, "UAV terrain following technology application in the mining subsidence monitoring research," *Bulletin of Surveying and Mapping*, vol. 05, pp. 111–115, 2021.

[29] Y. Wang, J. Wang, Y. Huang, F. Tian, and G. Chen, "Several key technologies and their applications for multi-source monitoring and analysis of surface hazards in mining areas," *Bulletin of Surveying and Mapping, S2*, no. S2, pp. 4–9+15, 2014.

[30] S. T. Henderson, M. E. Pritchard, J. R. Cooper, and Y. Aoki, "Remotely sensed deformation and thermal anomalies at mount pagan, mariana islands," *Frontiers of Earth Science*, vol. 7, p. 238, 2019.

[31] D. Müller, T. R. Walter, A. Schöpa et al., "High-resolution digital elevation modeling from TLS and UAV campaign reveals structural complexity at the 2014/2015 holuhraun eruption site, Iceland," *Frontiers of Earth Science*, vol. 5, 2017.

[32] Y. Chengsheng, Z. Qin, Z. Chaoying, J. I. Lingyun, and Z. Wu, "Monitoring mine collapse by D-InSAR," *Mining Science and Technology*, vol. 20, pp. 0696–0700, 2010.

[33] Y. Du, S. Yan, H. Yang, J. Jiang, and F. Zhao, "Investigation of deformation patterns by DS-InSAR in a coal resource-exhausted region with spaceborne SAR imagery," *Journal of Asian Earth Sciences*, vol. X5, Article ID p100049, 2021.

[34] W. Shi, X. Qu, C. Jiang, and K. Li, "Study on numerical simulation test of mining surface subsidence law under ultrathick loose layer," *Geofluids*, vol. 2021, Article ID 6655827, 10 pages, 2021.

[35] L. Xu, X. Zhou, X. Li, R. H. Jhaveri, T. R. Gadekallu, and Y. Ding, "Mobile collaborative secrecy performance prediction for artificial IoT networks," *IEEE Transactions on Industrial Informatics*, vol. 3128506, 2021.

[36] R. H. Jhaveri, S. V. Ramani, G. Srivastava, T. R. Gadekallu, and V. Aggarwal, "Fault-resilience for bandwidth management in industrial software-defined networks," *IEEE TRANSACTIONS ON NETWORK SCIENCE AND ENGINEERING*, vol. 8, no. 4, 2021.

[37] N. M. Balamurugan, S. Mohan, M. Adimoola, A. John, T. R Gadekallu, and W. Wang, "DOA tracking for seamless connectivity in beamformed IoT-based drones," *Computer Standards & Interfaces*, vol. 79, Article ID 103564, 2022.

[38] P. N. Srinivasu, A. K. Bhoi, R. H. Jhaveri, G. T. Reddy, and M. Bilal, "Probabilistic Deep Q Network for real-time path planning in censorious robotic procedures using force sensors," *Journal of Real-Time Image Processing*, vol. 18, no. 5, pp. 1773–1785, 2021.

[39] J. Wang, Y. Li, X. Zhou, L. Wu, and S. Wei, "Ground movement caused ByMiningunder thick alluvium," *Journal of China Coal Society*, vol. 01, 1997.

[40] Y. Liu, H. Dai, and W. Guo, "Surface movement laws of deep wide strip-pillar mining under thick alluvium," *Journal of Mining & Safety Engineering*, vol. 03, pp. 336–340, 2009.

[41] X. Chen, J. Su, and Z. Zhao, "Study of surface movement principle of coal seam mining under super thick unconsolidated stratum," *Coal Mining Technology*, vol. 03, pp. 59–61+77, 2017.

[42] Q. Li, C. Zhang, K. Li, S. Yu, Y. Cao, and T. Yang, "Analysis of the influence of different parameters of mining under super-thick loose layer on surface subsidence," *Coal Science and Technology*, vol. 49, no. 11, pp. 191–199, 2021.

[43] G. Xu, S. Xu, D. Li, and H. Li, "Field research on surface movement characteristic by coal mining under thick alluvium in Zhaogu mine area," *China Mining Magazine*, vol. 05, pp. 168–172, 2021.

[44] T. Li, H. Zhang, H. Fan, C. Zheng, and J. Liu, "Position inversion of goafs in deep coal seams based on DS-InSAR data and the probability integral methods," *Remote Sensing*, vol. 13, no. 15, p. 2898, 2021.

[45] H.-D. Fan, W. Gu, Y. Qin, J.-Q. Xue, and B.-Q. Chen, "A model for extracting large deformation mining subsidence using D-InSAR technique and probability integral method," *Transactions of Nonferrous Metals Society of China*, vol. 24, no. 4, pp. 1242–1247, 2014.

[46] Y. Xia and Y. Wang, "InSAR- and PIM-based inclined goaf determination for illegal mining detection," *Remote Sensing*, vol. 12, no. 23, p. 3884, 2020.

[47] S. Matloob, Y. Li, and K. Z. Khan, "Safety measurements and risk assessment of coal mining industry using artificial intelligence and machine learning," *Open Journal of Business and Management*, vol. 9, no. 3, 2021.